BEAM DIAGNOSTIC TECHNIQUES, OBSERVATIONS AND COMPARISON WITH THEORY

A. Hofmann
CERN
CH-1211 Geneva 23

Abstract Among the different methods of beam diagnostics available in modern storage rings three classes are presented here in some detail. The first two use the near-field of the beam measured by the position monitors. The optical functions - betatron phase advances and beta functions - are obtained by exciting a betatron oscillation and measuring its phase and amplitude at the beam position monitors around the ring. Modern read-out electronics, which memorize the readings taken in successive turns, are particularly well suited for this method. A second group of measurements is concerned with the properties of the beam itself. The frequency distribution of the particles can directly be deduced from the beam response to a harmonic excitation. Such measurements give also the beam stability and the impedance of the beam surroundings. The third class observes the far-field of the beam emitted as synchrotron radiation. Using this radiation for imaging or measuring its angular divergence gives the transverse beam dimensions.

1 Introduction

A wide range of diagnostic tools are available to make observation of the beam parameters and behavior in a storage ring. We will concentrate here on the most commonly used non-destructive devices, namely beam position intensity monitors and synchrotron light detectors. The beam position and intensity monitors have a wide range of applications. We will concentrate here on two representative examples. In the first case an excited betatron oscillation is observed in phase and amplitude at the different position monitors around the ring. Such a measurement allows to deduce the betatron phase advance between the observation points and the relative value of the beta functions at those locations. It can be used to check the optics of a machine. In a second example we measure the phase and amplitude of a beam oscillation with respect to the force which excites it. This observation serves to obtain information mainly about the beam itself but also about its interaction with the surroundings. The synchrotron radiation monitors give such information in a more direct way through a visual image of the beam cross section. In each of the three cases we discuss briefly the accuracy as well as the limitations of such measurements and compare the results with theoretical expectations. This will be done by giving particular examples in some detail which should be representative for a wide range of similar measurements. I would like to apologize for choosing mainly those cases where I am familiar with the details. The same or very similar experiments have been carried out at many other machines and are often part of every day operation.

2 Measuring betatron phase advances and relative beta functions

Measurement done with an unbunched beam

A betatron phase advance measurement is carried out with a coasting beam by exciting it with a frequency which is swept through a betatron side band

$$\omega_\beta = \omega_0(Q+n) \tag{1}$$

where ω_0 is the revolution frequency and Q is the betatron tune. The integer n goes through negative and positive numbers leading to frequencies with both signs. With the instruments positive frequencies are observed and the frequency ω_β gives an upper side band to the revolution frequency harmonics if $n > -Q$ and a lower side band if $n < -Q$. The resulting betatron oscillation is observed with two position monitors located at the azimuthal angles θ_1 and θ_2 of the ring. The signals are than compared for the relative phase and amplitude by a network analyzer which also provides the RF-signal for the beam excitation. Such an experimental set-up is shown in fig. 1 for the example of the ISR [1]. The beam monitors are sensitive to the dipole moment $D = yI_0$ of the circulating current I_0 having the displacement y. For an excited betatron oscillation of a coasting (unbunched) beam this dipole moment as a function of t and θ is given by

$$D(t,\theta) = \hat{y}I_0\sqrt{\frac{\beta(\theta)}{\beta(0)}}\cos\left(\omega_\beta t + \xi(\theta)\right), \tag{2}$$

with $\xi(\theta) = \phi(\theta) - \theta(Q+n)$, and where $\phi(\theta)$ is the betatron phase advance and $\beta(\theta)$ is the value of the beta function. By comparing the measured phase ξ of the signals from the two position monitors we are actually measuring

$$\Delta\xi = \xi(\theta_2) - \xi(\theta_1) = \phi(\theta_2) - \phi(\theta_1) - \Delta\theta(Q+n), \tag{3}$$

where $\Delta\theta = \theta_2 - \theta_1$. The desired phase advance $\Delta\phi$ between the two monitors is related to the measured phase difference $\Delta\xi$ of the signals by

$$\Delta\phi = \phi(\theta_2) - \phi(\theta_1) = \Delta\xi + \Delta(\theta)(Q+n). \tag{4}$$

For a real experiment we have to consider the finite length L of the cable connecting the monitor to the network analyzer in which the signals travel with the speed c'. It leads to a correction of the above relation

$$\Delta\phi = \Delta\xi + (Q+n)(\Delta\theta + \frac{\omega_0}{c'}(L_2 - L_1)). \tag{5}$$

A coasting beam has no time structure which could be used to calibrate the cable lengths. However the effect can be reduced by measuring the phase advance using two frequencies corresponding to different values of the integer n. This is specially advantageous to chose an adjacent upper and lower side band (also called fast and slow wave). While doing the phase measurement we can also compare the amplitudes D of the observed oscillation from which the ratio of the beta functions at the two locations can be obtained. The example exhibited in fig. 1 shows the lay-out and the pictures for the phase and amplitude displayed by the spectrum analyzer for the fast and slow wave. The obtained results for about one third of the ISR are shown by plotting the expression $\phi(\theta) - -Q\theta$ for the phase to keep the curve in a reasonable

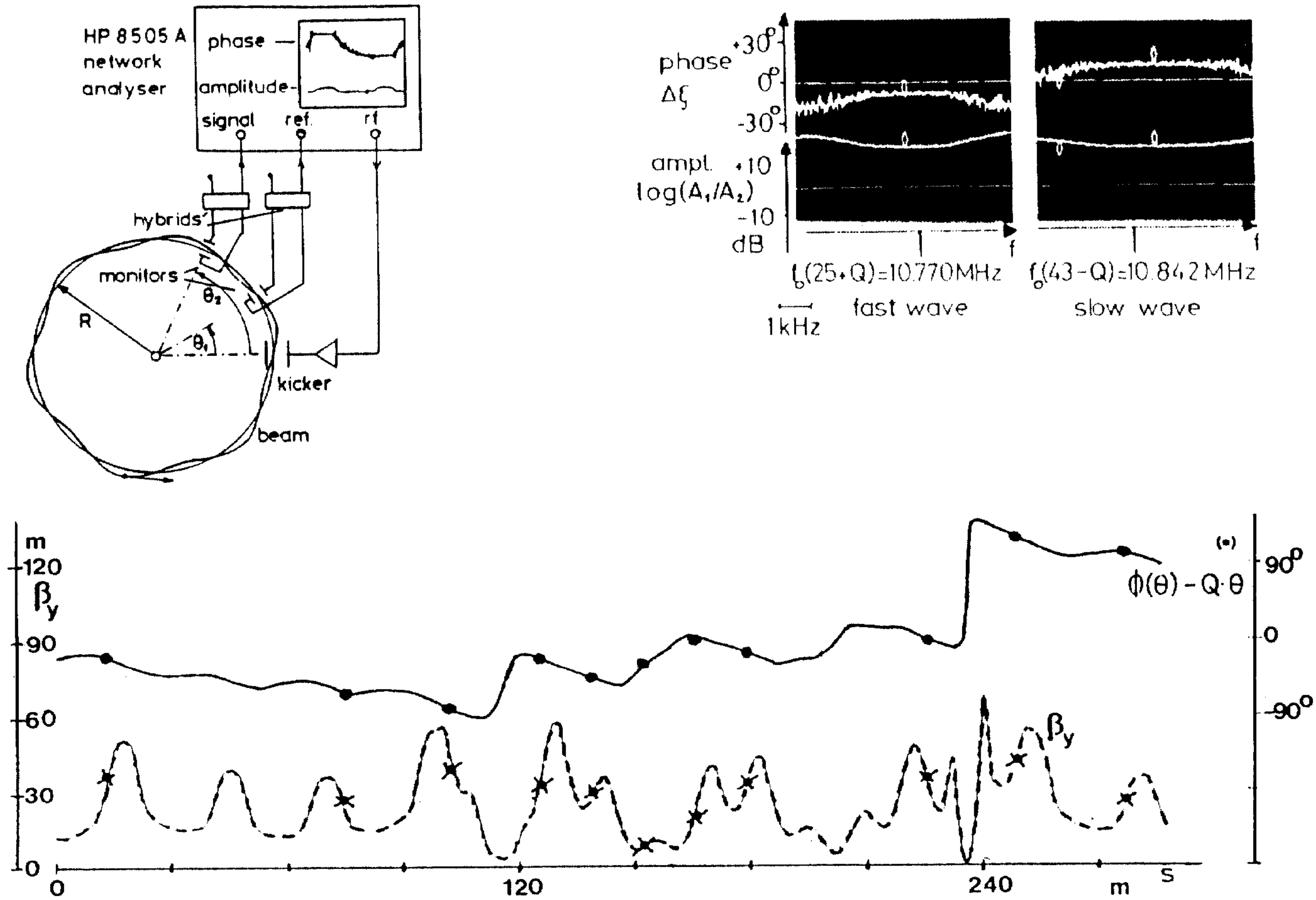

Figure 1: Measurement of the betatron phase advance in the ISR

vertical range. The relative beta functions measured have been normalized with the known average value. Both parameters are shown together with the calculated values. The agreement seen in this figure seems to be very good. A more detailed analysis gives an rms. deviation from the calculation of about 3^0 for the phase and about 11% for the beta function. The calculation is of course also not without error since the optics including orbit distortions at the sextupoles is known with limited accuracy only. The measurement errors were estimated to be about 3^0 for the phase and 10% for the beta functions. More accurate measurements have been done in the SPS [2] and at CESR [3].

Measurements done with a bunched beam

Measurements can be done with bunched beams using the same method. Since the beam provides now a timing signal the cable lengths can be can be calibrated easily. However, bunched beams allow to do this phase advance measurement in a more elegant way. The bunch intensity signal can be used to trigger the electronics of the position monitor to make a 'sample and hold' of its signal and store the result in a memory. After a measurement this memory contains beam positions which are no longer related to time but to the turn number. The phase advance measurement can now be carried out by kicking the beam and let it execute a free betatron oscillation. The signals from two or more position monitors are collected in the respective memories for a certain time. The stored data can then be Fourier analyzed to get the betatron frequency. Comparing two such analyses gives the measured phase $\Delta\xi$ between the signals from the two monitors from which the betatron phase advance is obtained directly. A phase advance measurement carried out at SPEAR [4] by this method is illustrated in fig. 2. Signals obtained from a pair of position monitors are directly displayed on a x-y plot giving a Lissajou figure of the oscillation for the cases of 12^0 and 270^0 phase advance between the monitors. The result of the phase measurement around the ring is shown and compared with the one calculated from the model of the machine optics with the two low beta insertions marked by a line. No difference between measurements and expectations can be seen on this scale. A detailed analysis indicates an average error of about 0.4^0.

Discussion

Phase measurements need relatively clean signals from the position monitors to allow a phase comparison at all. However, if this is fulfilled they are extremely accurate. Contrary to signal sizes, the phase is very little influenced by the geometry of the monitor or by amplifiers. The effect of the unknown cable length can be well corrected with the methods mentioned. Modern position monitors often digitize the signals directly and put them in a memory to be read by the control system [5]. Phase measurement by the digital method can now become a routine operation. They can be used to check the optics of a machine and to find and locate possible focussing errors. With the improved accuracy it might be possible to also measure the chromatic functions like $d\phi/dp$ by carrying out experiments at

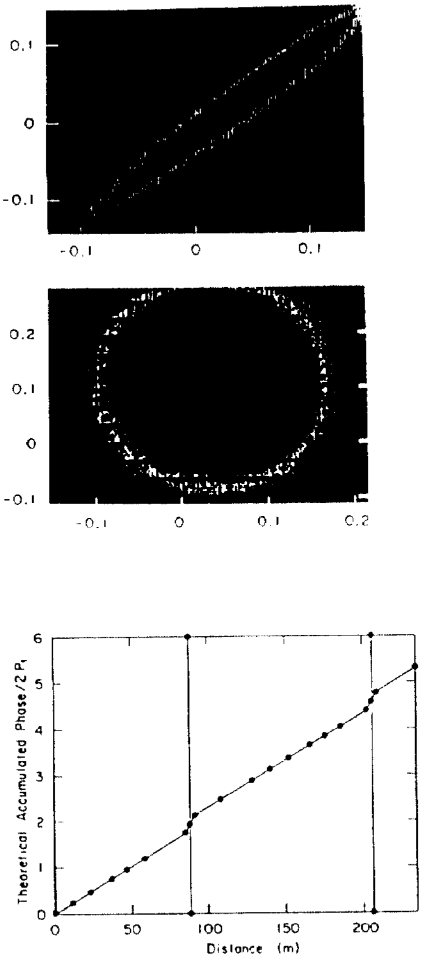

Figure 2: Bunched beam phase advance measurement in SPEAR [4]

different momenta Δp of the beam. If we had a position monitor at each quadrupole the phase measurement would allow to reconstruct the beta function within a short lens approximation all around the ring. One important area where the phase measurement is not sufficiently accurate is the investigation of low beta sections. Here, the phase advance is always close to π and depends only weakly on the value of the beta function in the interaction point once it is small. Measurements of tune variation versus quadrupole strengths have to be done in addition.

3 Beam transfer function

Response of a coasting beam to transverse excitation

This measurement uses a very similar set-up and the same instrumentation as the phase measurement of a coasting beam described before. However we compare now not the signals from different monitors but relate the response with the excitation. We consider now a coasting beam with a certain distribution of its particles in momentum $dN/dp = F_p(\Delta p)$, where $\Delta p = p - p_0$ is the deviation from a certain central momentum p_0. Particles with different momenta will in general also have different betatron frequencies $\omega_\beta = \omega_0(Q+n)$ as observed by a stationary monitor due to two effects: the dependance of the revolution frequency ω_0 on momentum through the momentum compaction factor α and the dependance of the tune Q on momentum through the chromaticity

$$\Delta\omega_0 = \omega_0(\alpha - 1/\gamma^2)\frac{\Delta p}{p}\ ,\ \Delta Q = \frac{1}{p}\frac{dQ}{dp}\frac{\Delta p}{p} = Q'\frac{\Delta p}{p}. \quad (6)$$

giving

$$\Delta\omega_\beta = (Q' - (\alpha - 1/\gamma^2)(Q+n))\omega_0\frac{\Delta p}{p}. \quad (7)$$

Through this relation the distribution $F(\Delta\omega_\beta)$ in the betatron frequency can be obtained from $F_p(\Delta p)$ through a simple linear scaling. It is important to note that for this case of a coasting beam this distribution is given by external parameters and the momentum and does not depend on the betatron amplitude we will excite.

We will now apply a harmonic transverse acceleration with frequency ω to the beam and excite a betatron oscillation. We consider first the response of a narrow ring of particles having the same momentum and start with the equation of motion in the vertical coordinate y [6]

$$\frac{d^2y}{dt^2} + \omega_0^2 Q^2 y = \hat{G}e^{-i\omega t} \quad (8)$$

We seek a solution which look for a stationary observer as a wave $y = \hat{y}\exp(i(n\theta - \omega t))$. Using $dy/dt = i(n\omega_o - \omega)y$ we get

$$\frac{\hat{y}}{\hat{G}} = \frac{-1}{(\omega - \omega_{\beta,s})(\omega - \omega_{\beta,f})}, \quad (9)$$

where we introduced the slow and fast wave betatron frequencies $\omega_{\beta,s} = \omega_0(Q-n)$ and $\omega_{\beta,f} = \omega_0(Q+n)$ and assumed that the beam is observed close to the kicker ($\theta = 0$). The response will only be large if the exciting frequency ω is close to either the slow or the fast wave betatron frequency. Taking the first case we get

$$\frac{\hat{y}}{\hat{G}} \sim \frac{1}{2Q\omega_0}\frac{1}{\omega - \omega_{\beta,s}}. \quad (10)$$

We consider now the particle distribution in $\omega_{\beta,s}$ and calculate the center of mass motion by forming the weighted average of the single particle response

$$\begin{aligned} <\hat{y}> &= \frac{\hat{G}}{2Q\omega_0 N}\int\frac{F(\omega_{\beta,s})}{\omega - \omega_{\beta,s}}d\omega_{\beta,s} \\ &= \frac{\hat{G}}{2Q\omega_0 N}\left[PV\int\frac{F(\omega_{\beta,s})}{\omega - \omega_{\beta,s}}d\omega_{\beta,s} \pm i\pi F(\omega)\right]. \quad (11)\end{aligned}$$

The limits of the integral have to cover the distribution of the side band of interest. The integration covers a pole which leads to the residue the sign of which is not determined. The reason for this is the fact that we have not specified the initial conditions and the integral includes the possibilities of growing or decaying oscillations. This becomes clearer by differentiating the above equation and comparing the velocity $\dot{y} = -i\omega y$ of the response with the acceleration G

$$<\hat{\dot{y}}> = \frac{\hat{G}\omega}{2Q\omega_0 N}\left[\pi F(\omega) - iPV\int\frac{F(\omega_{\beta,s})}{\omega - \omega_{\beta,s}}\right]. \quad (12)$$

The first term of the right hand side of this equation is real and positive which means that the velocity $\dot{y}$ and the acceleration G are in phase and energy is absorbed by the beam. The second term is imaginary, meaning that velocity and acceleration are out of phase. From the point of view of diagnostics the first term is most important since it gives directly the particle distribution $F(\omega_{\beta,s})$ in incoherent betatron frequency $\omega_{\beta,s}$ which in turn is related to the momentum distribution of the particles. To make the above expression more suitable for application we introduce the FWHM betatron frequency spread S in the beam and normalize with it the frequencies $\xi_\beta = \omega_{\beta,s}/S, \xi_0 = \omega/S$ as well as the distribution $f(\xi_\beta) = SF(\omega_{\beta,s})/N$. Furthermore we normalize the response by multiplying with factors which are approximately constant.

$$\begin{aligned} R_0 &= \frac{2Q\omega_0 S}{\omega}\frac{<\hat{y}>}{\hat{G}} = -2iQS\frac{<\hat{y}>}{G} = -i\int\frac{f(\xi_\beta)}{\xi_0-\xi_\beta}d\xi_\beta \\ &= \pi f(\xi_0) - iPV\int\frac{f(\xi_\beta)}{\xi_0 - xi_\beta}d\xi_\beta. \qquad (13) \end{aligned}$$

Before we go to examples we have to consider the influence of the impedance of the beam surroundings. In the presence of a transverse impedance $Z_T(\omega)$ the oscillating beam will introduce fields in the impedance which apply an additional force to the beam. The acceleration G contains now an external part due to the excitation by our applied signal and an additional part due to the impedance [6]

$$G = G_{ext} - i\frac{eI_0 Z_T(\omega) <\hat{y}>}{2\pi R\gamma m_0}. \qquad (14)$$

We are only interested in the ratio between the beam oscillation and the external acceleration. Including the effect of the impedance we get for the inverse of the normalized response

$$\frac{1}{R} = \frac{1}{R_0} - \frac{ecI_0 Z_T}{4\pi\gamma m_0 c^2 QS}. \qquad (15)$$

The impedance shifts the inverse response by an amount proportional to $-Z_T$. We will now discuss the experiment outlined in fig. 3. The beam is transversely excited with a frequency swept through a lower betatron side band of a coasting beam. The response is compared to the exciting signal in phase and relative amplitude as shown on the network analyzer display. To make the shift of the inverse response visible the second term on the right hand side of (15) is varied by changing the spread S through Q' (7). This inverse response is plotted as the real part against the imaginary part in fig. 3 for the different values of Q'. It can be clearly seen that the curve gets shifted more and more with decreasing Q'. To check the form of the curve the particle distribution in momentum $F_p(\Delta p)$ has been obtained from a longitudinal Schottky scan and the particle distribution $F(\omega_{\beta,s})$ calculated from the relation (7). From this the inverse response in absence of impedance has been computed and plotted in fig. 3. It has with quite good accuracy the same form as the measured inverse responses but is of course not shifted. From the measured shift the transvere impedance has been determined. It is show at the bottom of fig. 3. For the resistive part it agrees well with the expected resistive wall impedance at low frequencies. The reactive part has in addition a constant inductance consistant with observations by other methods.

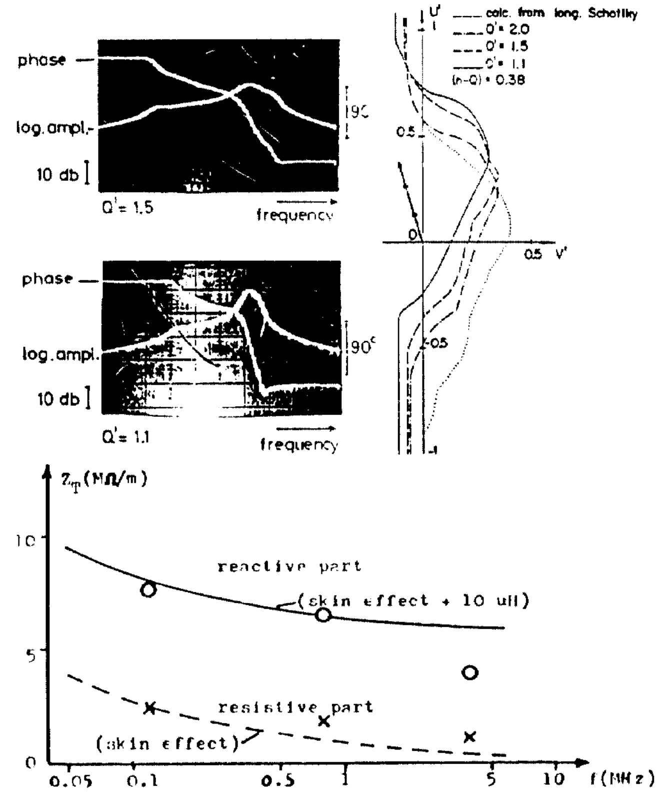

Figure 3: Measurement of the transverse response of a coasting beam

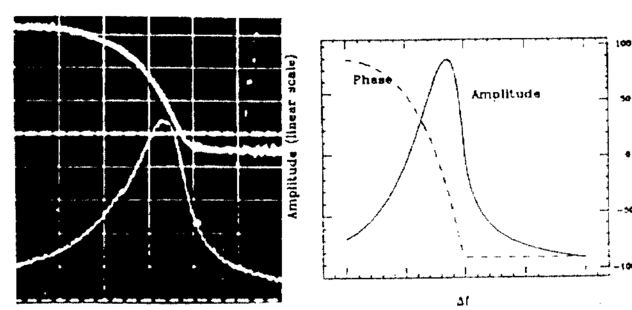

Figure 4: Measurement of the quadrupole mode transfer function

Response of a bunched beam to a longitudinal excitation

We are going now to a bunched beam and consider longitudinal excitation of dipole and quadrupole oscillation which can be done by phase or amplitude modulation the RF-voltage. The situation is considerably more complicated than in the case treated in the previous subsection. The frequency spread is now given by the amplitude dependence of the synchrotron frequency in the non-linear rf-bucket. We will not give any derivations here but refer to publications on this subject [7,8,9] and give only the results. It can be shown that for a stationary bunch the particle distribution is a function of the Hamiltonian H only and is of the form $g(H)$. The synchrotron frequency $\omega_s(H)$ will also be a function of the Hamiltonian. The beam response R_d for the dipole and R_q for the quadrupole mode can then be written

$$R_d = C_d\int_0^\infty \frac{\frac{dg(H)}{dH}H}{\omega - \omega_s(H)}dH\ , \ R_q = C_q\int_0^\infty\frac{\frac{dg(H)}{dH}H^2}{\omega - 2\omega_s(H)}dH. \qquad (16)$$

The response of the quadrupole mode measured at SPEAR at relatively low current is shown in fig. 4 and compared qualitatively with the calculation. The agreement is quite good. At larger currents the effect of the impedance becomes important. It will lead to a shift of the inverse response but will at the same time alter the Hamiltonian and the frequency distribution which makes the measurements complicated [10].

Discussion of the beam transfer function

For coasting beams the beam transfer function is relatively easy to measure since the undisturbed beam does not produce any large signals in the monitors. The particle distribution and the low frequency impedance can be measured well. As a special application feed-back systems can be checked by observing the shift of the inverse response when the system is turned on. Bunched beams give large common mode signals which make the measurement of the beam response more difficult. In addition the form of the transfer function is more complicated and the impedance will change the frequency distribution. In such cases the beam response to a kick might often be a more direct measurement of properties like beam stability.

4 Investigating the beam with synchrotron radiation

Imaging of the beam cross section

In nearly all electron machines one forms an image of the beam by using the visible part of the radiation to form an image of the beam cross section with a lens. It is interesting to note that due to the small natural vertical opening angle ψ_{rms} on

$$\psi_{rms} \sim \frac{1}{\gamma}\left(\frac{\lambda}{\lambda_c}\right)^{1/3} \sim \left(\frac{\lambda}{\rho}\right) \tag{17}$$

diffraction is relatively important and limits the resolution to

$$r \sim \lambda^{2/3}\rho^{1/3} \tag{18}$$

where λ is the wave length of the radiation used, λ_c the critical wave length and ρ the radius of curvature. For large machines like LEP the above expression indicate a resolution of about 0.5 mm which is not sufficient. Going to shorter wave lengths or a locally smaller bending radius helps. Furthermore the source point of the radiation should be located at a large value of the beta function.

Observing the angular divergence of the emitted radiation

This method is less widely used and will be illustrated in more detail. The divergence of the radiation consists basically of two parts, the natural divergence of the radiation mentioned above and the angular divergence of the electron beam we want to measure. Clearly the optimum source location is a place with a small value of the beta function. Using synchrotron radiation from bending magnets this method will only give information about the vertical beam emittance. However, the radiation from undulator allows measurements of both planes. We will discuss such an experiment done at PEP [11] A plane, harmonic undulator with $N_u = 26$ periods of length $\lambda_u = 77$ mm was used. The emitted radiation went through a monochromator tuned to the fundamental frequency of the undulator, fig. 5. At the end of this beam line, $L = 58$ m from the source the size of the photon beam was measured. It can be shown [11] that the natural rms. width of the monochromatized undulator radiation is given by

$$\theta_{\gamma-rms} = \frac{1}{\gamma}\sqrt{\frac{3}{4\pi N_u}} \tag{19}$$

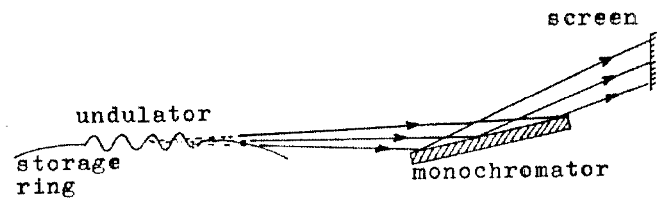

Figure 5: Measurement of the PEP emittance with undulator radiation

The photon beam size due to the finite emittance ϵ of the electron beam can be obtained by extending the lattice functions $\beta(0), \alpha(0)$ and $\gamma(0)$ at the source to the screen at the distance L where the photon beam size is measured by [12]

$$\beta(L) = \beta(0) - 2\alpha(0)L + \gamma(0)L^2.$$

This gives for the contribution of the emittances to the photon beam size $\sigma_{x\beta} = \sqrt{\epsilon_x\beta_x(L)}$ and $\sigma_{y\beta} = \sqrt{\epsilon_y\beta_y(L)}$. For the horizontal plane there is also a contribution from the dispersion at the source point. Subtracting quadratically the contribution due to the natural opening angle of the undulator radiation, due to the dispersion and due to the resolution of the measurement device from the measured beam size the contribution due to the emittances and the emittances themselve can be determined. For the PEP experiment the following results were obtained for the uncoupled emittance $\epsilon_0 = \epsilon_x + \epsilon_y$ For the normal lattice at 14.5 GeV the measurement gave 86 nm rad while 117 nm rad were expected. For the low emittance lattice at 8 GeV the measurement gave 13.3 nm rad while 9.9 nm rad were expected. The discrepancies between measured and calculated values can probably be caused by the errors in the lattice functions at the sources.

References

[1] J. Borer et al. Proc. of the 1983 Particle Accel. Conf., IEEE trans. on Nucl. Sci. NS 20-3, (1983) 2483.

[2] R. Bossart, W. Scandale; Proc. 1987 IEEE Particle Accelerator Conference (1987) 760.

[3] D. Rice; private communication.

[4] P.L. Morton et al.; 1987 IEEE Particle Accel. Conf. (1987) 1367.

[5] J. Borer et al.; 1987 IEEE Particle Accel. Conf. (1987) 778.

[6] A. Hofmann, B. Zotter; Proc. of the 1977 Particle Accel Conf., IEEE Trans. on Nucl. Sci.,NS-24 (1977) 1487.

[7] H.G. Hereward; CERN/MPS/DL 69-11 (1969).

[8] R. Boni et al. LNF-Div. Report, RM-23, 1981.

[9] D. Boussard; CAS CERN Accel. School 1985, CERN 87-03 (1987 416.

[10] J.M. Jowett et al.; contribution to this conference.

[11] G. Brown et al.; Proc. 1987 IEEE Particle Accel. Conf. (1987) 461.

[12] M. Placidi; private communication 1985.